doi: 10.14735/amcsnn2017700

Quantitative MRI Texture Analysis in Differentiating Enhancing and Non-enhancing T1-hypointense Lesions without Application of Contrast Agent in Multiple Sclerosis

Kvantitativní analýza MRI textury pro rozlišení enhancujících a neenhancujících T1 hypointenzních lézí bez podání kontrastní látky u roztroušené sklerózy

Abstract

Aims: The aim of this study was to evaluate texture analysis (TA) in pre-contrast injection MR images to improve accuracy and to identify subtle differences between enhancing lesions (ELs), non-enhancing lesions (NELs) and persistent black holes (PBHs). *Materials and methodology:* The MR image database comprised 90 patients; 30 of whom had only PBHs, 25 had only ELs and 35 neither EL or PBH. These were assessed by the proposed TA method. Up to 300 statistical texture features were extracted as descriptors for each ROI/lesion. Differences between the lesion groups were analyzed and evaluations were made for area under the receiver operating characteristic curve (A_z) for each significant texture feature. Linear discriminant analysis (LDA) was employed to analyze significant features and increase power of discrimination. *Results:* At least 14 texture features showed significant difference between NELs and ELs, NELs and PBHs, and ELs and PBHs. By using all significant features, LDA indicated a promising level of performance for classification of NELs and PBHs with A_z value of 0.975 that corresponds to sensitivity of 94.3%, specificity of 96.3%, accuracy of 95.5%. In classification of ELs and NELs (or PBH), LDA demonstrated discrimination performance with sensitivity, specificity and accuracy of 100% and A_z of 1. *Conclusions:* TA was determined as a reliable method, with potential for characterization and the method can be applied by physicians to differentiate NELs, ELs and PBH in pre-contrast injection MRI imaging.

Souhrn

Cíle: Cílem této studie bylo zhodnotit analýzu textury (AT) na snímcích MR před podáním kontrastní látky z hlediska zlepšení přesnosti a rozlišení jemných rozdílů mezi enhancujícími lézemi (EL), neenhancujícími lézemi (NEL) a perzistentními černými dírami (persistant black holes; PBH). *Materiál a metodika:* Databáze zobrazení MR zahrnovala 90 pacientů, z nichž 30 mělo pouze PBH, 25 mělo pouze EL a 35 nemělo ani EL ani PBH. Tato zobrazení byla zhodnocena pomocí navrhované metody AT. Bylo extrahováno na 300 statistických texturních znaků jako deskriptorů každého ROI/léze. Byly analyzovány rozdíly mezi skupinami lézí a byla změřena plocha pod křivkou (A_z) pro každý významný texturní znak. K analýze signifikantních znaků a ke zvýšení síly odlišení byla použita lineární diskriminantní analýza (LDA). *Výsledky:* Nejméně 14 texturních znaků prokázalo významný rozdíl mezi NEL a EL, NEL a PBH a EL a PBH. Při použití všech významných znaků naznačila LDA slibnou schopnost klasifikace NEL a PBH s hodnotou A_z 0,975, která odpovídá senzitivitě 94,3 %, specificitě 96,3 % a přesnosti 95,5 %. U klasifikace EL a NEL (nebo PBH) prokázala LDA diskriminační výkon odpovídající senzitivitě, specificitě a přesnosti 100 % a A_z 1. *Závěry:* AT byla vyhodnocena jako spolehlivá metoda s potenciálem charakterizovat NEL, EL a PBH a jako metoda, kterou mohou lékaři použít k rozlišení NEL, EL a PBH na snímcích MR před podáním kontrastní látky.

The authors declare they have no potential conflicts of interest concerning drugs, products, or services used in the study.
Autoři deklarují, že v souvislosti s předmětem studie nemají žádné komerční zájmy.
The Editorial Board declares that the manuscript met the ICMJE "uniform requirements" for biomedical papers.
Redakční rada potvrzuje, že rukopis práce splnil ICMJE kritéria pro publikace zasílané do biomedicínských časopisů.

A. A. Ardakani[1], S. M. Nabavi[2], A. Farzan[3], B. K. Najafabad[1]

[1] Department of Medical Physics, School of Medicine, Iran University of Medical Sciences, Tehran, Iran
[2] Neurology Group, Regenerative Medicine Department, Stem Cell Biology and Technology, Center for Neuroscience and Cognition, Royan Institute, Tehran, Iran
[3] Department of Neurosurgery, School of Medicine, Shahed University, Tehran, Iran

✉
Seyed Massood Nabavi
Fellowsip of Multiple Sclerosis
Center for Neuroscience and Cognition, Royan Institute
Tehran, Iran
e-mail:
seyedmassoodnabavi@gmail.com

Accepted for review: 8. 3. 2017
Accepted for print: 11. 7. 2017

Key words

contrast media – diagnosis – magnetic resonance imaging – multiple sclerosis – neurogenic inflammation – pattern recognition

Klíčová slova

kontrastní média – diagnóza – magnetická rezonance – roztroušená skleróza – neurogenní zánět – rozlišování vzorců

Introduction

Multiple sclerosis (MS) is an immune-mediated disease of the central nervous system that affects mostly young adults [1]. Since 1980s magnetic resonance imaging (MRI) has been the most frequently used technique for evaluating MS lesions in the brain and spinal cord and to monitor progress of the disease [2,3]. An abnormal signal derived from an MS lesion may be caused by demyelination and increased water content of the brain in the vicinity of the lesion due to breakdown in the blood brain barrier [4]. These changes and destruction in the matrix and lesion material can affect image by increasing inherent time (relaxation and recovery time).

T2-weighted (T2WIs) and gadolinium--enhanced T1-weighted images (T1WIs) are sensitive methods that are used to monitor disease activity in subjects with MS [5,6]. The majority of new lesions will become enhanced and usually persist for 2–6 weeks [7]. Approximately 65–80% of contrast-enhancing lesions (ELs) initially appear as hypo-intense on T1WIs. Less than 40% of these lesions will persist and become chronic, resulting in a condition termed persistent black hole (PBH). The remaining 40% of enhancing lesions gradually return to isointense state due to remyelination and resolution of edema [8]. EL is a sensitive indicator of active inflammation and it impairs a patient's clinical status. PBHs also yield important information on areas of axonal loss and are associated with disability [5,6,9,10].

Conventional MRI does not detect microscopic tissue changes and it has been indicated that the details are not visible to the human eye [11]. An MR image comprises diverse gray-level intensity, and various tissue types have different textures. Texture of images describes complex visual patterns; show arrangements of structures or sub-patterns and distribution of pixel intensities within an image domain [12,13]. At times, patterns within an image may be different, but this may not be detected by the human eye. Although a human can achieve texture in qualitative terms, mathematically defined texture properties require quantitative texture analysis (TA). TA can detect pathological differences that cannot be perceived by the human eye using conventional brain imaging MRI [11]. This mathematical technique increases quantification of and information about lesions in the brain that would be undetectable by conventional measurements of lesion volume, intensity and shape [14].

Recent studies have employed TA to 1 – differentiate between lesions, normal white matter and normal appearing white matter [11,15–18]; 2 – differentiate between ELs and non-enhancing lesions (NELs) [19–21] and between transient and persistent black holes (PBH) [22]; 3 – follow up therapeutic response in MS patients [23]; 4 – correlate MRI texture with tissue pathology [24]; this study provides additional information in support of this method.

Previous studies have indicated different texture features between PBHs and transient black holes and between ELs and NELs on a T2WI. Hence active inflammatory or axonal destruction can affect the texture of a brain MRI. The aim in this study was to evaluate texture using a non-invasive method of detecting changes in ELs, NELs and PBHs on brain MRI image in MS patients. To the best of our knowledge, this is the first study to apply TA to evaluate differences between ELs, NELs and PBHs.

Methods

Patients and MRI acquisition

MS evaluation is generally based on conventional MRI imaging, following the McDonald criteria 2010 [25]. MS patients with at least two attacks of neurological deficit, with clinical or paraclinical evidence of involvement of two different regions in the brain, optic nerve or spinal cord were selected. Exclusion criteria included steroid treatment as it may strongly suppress appearance of ELs, and individuals who were alcoholics and/or smokers to avoid potential confusion [26,27].

Ninety patients (27 males and 63 females) including 80 relapsing-remiting MS (RRMS), 3 primary progressive MS (PPMS) and 7 secondary progressive MS (SPMS) were recruited for participation in this study, they were aged 35.41 ± 9.84 (mean age ± standard deviation) with MS confirmed by a neurologist. These patients were divided into three groups: 39 patients (11 males and 28 females aged 34.72 ± 9.23) had MS lesions with no ELs or PBHs, 32 patients (9 males and 23 females aged 35.31 ± 10.11) had PBHs only and 19 patients (7 males and 12 females aged 39.43 ± 9.82) had ELs only. To detect PBHs, we reviewed each patient's imaging within the past 1 year.

T2WIs of each patient were acquired with a 1.5-T Siemens Trio scanner (Siemens, Erlangen, Germany) using the turbo spin echo sequence (TR = 4500 ms, TE = 100 ms, number of excitations (NEX) = 2, matrix = 512*512, field of view (FOV) = 23 cm, slice thickness = 5 mm and inter-slice gap = 0.5 mm).

The imaging protocol included T1-weighted spin-echo imaging (TR = 400 ms, TE = = 11 ms, NEX = 2, matrix = 512*512, FOV = = 23 cm, slice thickness = 3 mm and inter-slice gap = 0.5 mm). Patients received 0.1 mmol/Kg paramagnetic agent (Dotarem®, Sanofi, Aulnay-sous-Bois, France). Post-contrast MR images were obtained 7 min after the injection.

Texture feature and regions of interest selection

MR image was inputted in the MaZda software (version 4.6, Institute of Electronics, The Technical University of Lodz, Poland) for TA. In general, 116 ROIs consisting of 54 NELs, 27 ELs and 35 PBHs were selected for discrimination and classification. All lesions were chosen in correspondence to the regions of post-contrast MRI images (Fig. 1). Up to 300 texture features were extracted that, based on Histogram (histogram distribution of the image), Absolute gradient (describes local distribution of grey level differences and spatial variation of grey--level values), Run-length matrix (Run length matrix p (i) represent the number of times there is a run of length "j" with intensity "i", i.e. Run length matrix counts of pixel runs with the specified gray-scale value and length in a given direction), Co-occurrence matrix (information about the distribution of pairs of pixels separated by a given distance and direction, i.e. represent the second order image histogram that contains probabilities of co-occurrence of pixel pairs with a given distance d (1, 2, 3, 4 and 5) and direction θ (0, 45, –45 and 90 degree) in image intensity levels Ng), Auto-regressive model (based on this model, image pixels have an interaction with surrounded pixels. Therefore, pixel intensity is a weighted sum of neighbouring pixel intensities), and Wavelets (analyze natural nonstationary signals and be localized in both spatial and frequency domains. Wavelets decompose the image signals into frequency components using independent spatially oriented frequency filters cascaded in a pyramidal structure) [12,28].

Statistical analysis

Data were tested for normality by the Kolmogorov–Smirnov test. One-way analysis of variance (ANOVA) was used to assess differences between groups (NEL, EL and PBH).

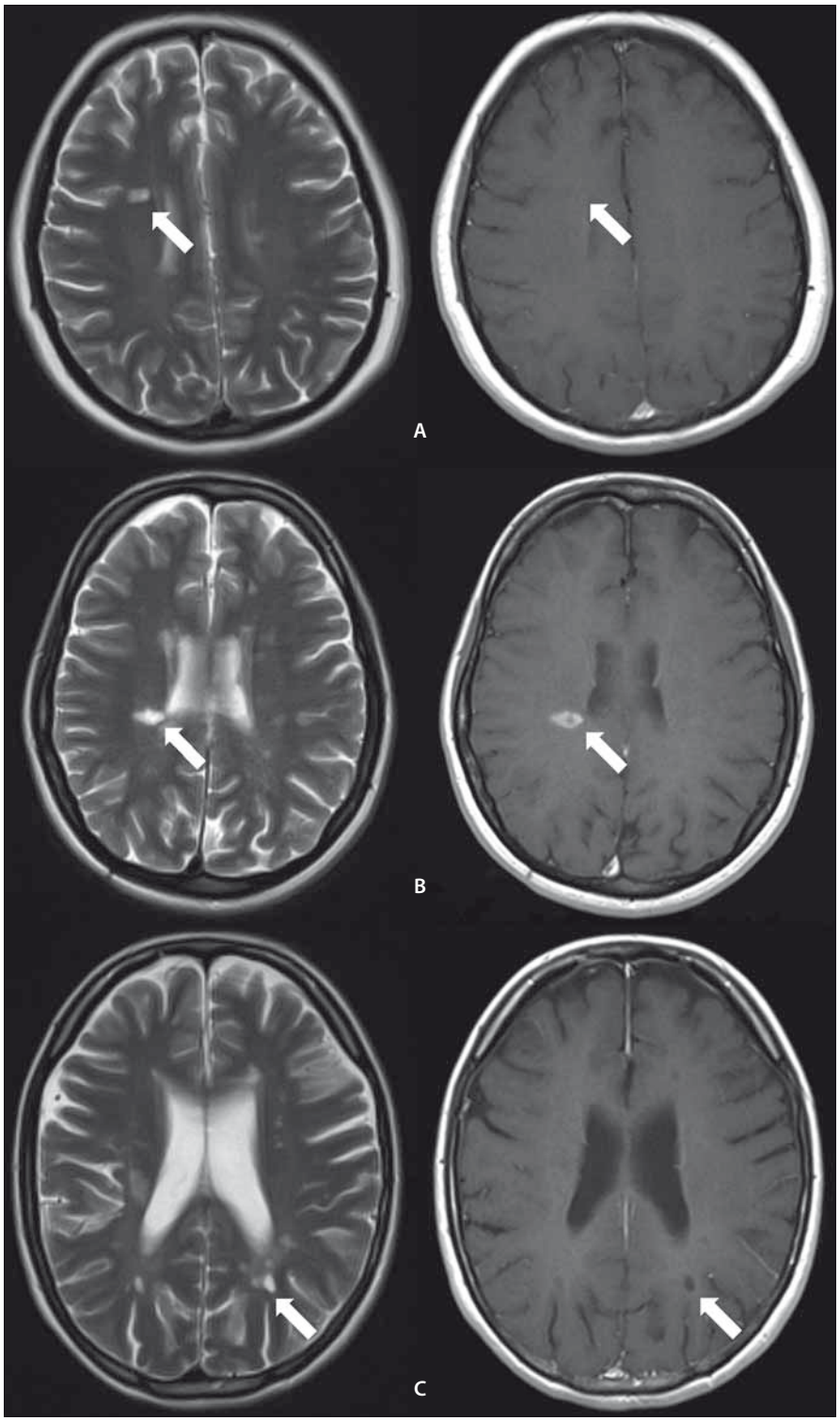

Fig. 1. Sample of NEL, EL and PBH lesions on T2WI. All lesions on T2WI (left) were selected according to post-contrast corresponding (right) to NEL (A), EL (B) and PBH (C).

For significant texture features, post hoc Scheffe or Tamhane's T2 test was applied to compare between groups. A P-value of < 0.05 was considered significant. An area under the receiver operating characteristic (ROC) curve (A_z) was calculated for each significant texture feature in order to evaluate overall performance of classification between the groups [29]. A_z values were estimated beyond the 95% confidence level.

Texture analysis and classification

Texture features that showed significant difference between the two groups were used for computerized multi parameter TA (MPTA) method. Linear discriminant analysis (LDA) was used to transform raw texture features to lower-dimensional spaces and to increase discriminative power; LDA seeks the most efficient directions for maximal separation of features. LDA demonstrated that variability among feature vectors of the same class (within class scatter) was minimized and variability among the feature vectors of different classes (between class scatter) was maximized. Features processed by LDA were considered useful for pattern recognition and classification as they put data of the same class closer together and data of different classes further apart. First nearest neighbor (1-NN) classifier was used for features resulting from LDA.

In order to compare performance of diagnostics, three well-known indexes were calculated: accuracy (ACC), sensitivity (SEN) and specificity (SPC). Their definitions are given as:

$$(1)\ Accuracy\ (ACC) = \frac{N_{TN} + N_{TP}}{N_{TN} + N_{FN} + N_{TP} + N_{FP}}$$

$$(2)\ Sensitivity\ (SEN) = \frac{N_{TP}}{N_{TP} + N_{FN}}$$

$$(3)\ Specificity\ (SPC) = \frac{N_{TN}}{N_{TN} + N_{FP}}$$

Where N_{TP} and N_{TN} are the number of true positive and true negative cases, respectively. N_{FP} and N_{FN} are the number of false positive and false negative cases, respectively. In this study, classification was performed between 1. NELs and ELs (positive – EL, negative – NEL); 2. NELs and PBH (positive = PBH, negative – NEL) and 3. ELs and PBHs (positive – EL, negative – PBH). An A_z value was also calculated to evaluate overall performance of the proposed MPTA method. A_z values were estimated beyond the 95% confidence level. Fig. 2 shows the CAD processing steps.

Results

Texture feature changes between groups

NELs vs. ELs

In general, 116 ROIs consisting of 54 NELs, 27 ELs and 35 PBHs were selected for statistical analysis and classification.

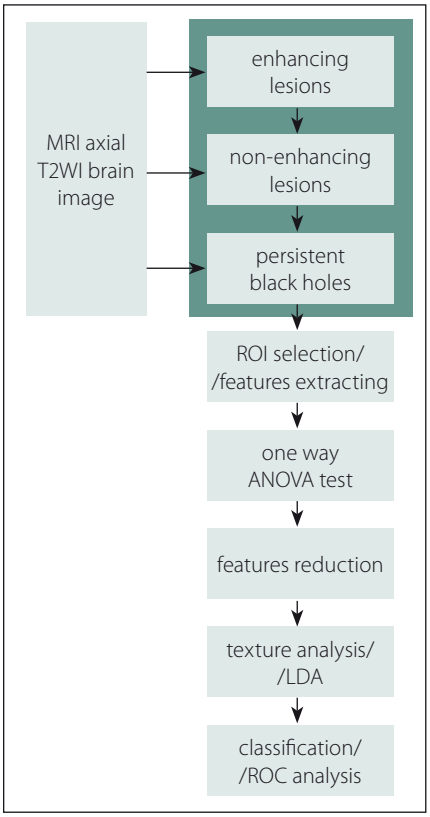

Fig. 2. Overview of texture analysis process on brain MRI images.

Tab. 1. Summary of performance for significant texture features in classification of NELs and ELs and the associated P-values.

Texture Features	Post Hoc Tests (P-value)	A_z value[a]
Correlat_S(1,-1)	P < 0.001	0.870 (0.794, 0.945)
ASMS(5,0)	P < 0.001	0.868 (0.777, 0.958)
WavEnHH_s-1	P < 0.001	0.859 (0.754, 0.965)
ASM_S(1,-1)	P < 0.001	0.826 (0.725, 0.928)
Correlat_S(1,1)	P < 0.001	0.822 (0.729, 0.916)
Mean	P < 0.001	0.822 (0.693, 0.950)
Gr_nonzeros	P < 0.001	0.806 (0.686, 0.925)
SE_S(1,0)	P < 0.001	0.805 (0.701, 0.909)
DV_S(0,1)	P < 0.001	0.802 (0.690, 0.915)
WavEnLL_s-2	P < 0.001	0.787 (0.654, 0.921)
Correlat_S(1,0)	P < 0.001	0.776 (0.678, 0.875)
WavEnLH_s-1	P < 0.001	0.774 (0.657, 0.892)
SRE_45Dgr	P < 0.001	0.766 (0.640, 0.893)
Gr_Kurtosis	P = 0.015	0.748 (0.618, 0.879)
RLNU_Vert	P < 0.001	0.729 (0.619, 0.840)
WavEnLH_s-2	P < 0.001	0.727 (0.593, 0.861)
Correlat_S(0,2)	P = 0.008	0.691 (0.555, 0.827)
SRE_Horz	P = 0.012	0.667 (0.512, 0.821)

A_z – area under ROC curve; ASM – indicates angular second moment; Gr_nonzeros – non-zero gradient matrix; SE – sum entropy; DV – difference variance; WavEnHH, WavEnLL and WavEnLH – 'high-high', 'low-low' and 'low-high' energy components in wavelet decomposition respectively; SRE_45Dgr and SRE_Horz – short sun emphasis in 45-degree and horizontal direction respectively; Gr_Kurtosis – kurtosis of absolute gradient; RLNU_Vert – run length non-uniformity in vertical direction; [a] numbers in parentheses are 95% CI.

Eighteen texture features showed significant difference between NELs and ELs: Correlation S(1,-1) (Correlat_S(1,–1)), Correlat_S(1,1), Correlat_S(1,0), Correlat_S(0,2), Angular second moment S(5,0) (ASM_S(5,0)), ASM_S(1,-1), Difference variance S(0,1) (DV_S(0,1)) and Sum Entropy S(1,0) (SE_S(1,0)) from Co-occurrence matrix Where S(i, j) shows the direction of matrix construction and inter pixel distance i along rows and j along columns of the matrix; 'high-high' energy components in first level wavelet decomposition (WavEnHH_s-1), 'low-high' energy components in first level wavelet decomposition (WavEnLH_s-1), WavEnLL_s-2 and WavEnLH_s-2 from Wavelet; Non-zero gradient matrix (Gr_nonzeros) and Kurtosis of absolute gradient (Gr_Kurtosis) from Gradient; Short Run Emphasis in Horizontal direction (SRE_Horz) and in 45-degree direction (SRE_45Dgr) Run Length Non-Uniformity in Vertical direction (RLNU_Vert) from Run-length matrix and Mean from Histogram (Tab. 1).

NELs vs. PBHs

Fourteen texture features showed significant difference between NELs and PBHs: WavEnLL_s-1,WavEnLL_s-2,WavEnLH_s-2fromWavelet; Mean from Histogram; Non-zero gradient matrix (Gr_nonzeros) from Gradient; Sum Average S(3–3) (SA_S(3–3)), SA_S(3,3), SA_S(3,0), Sum Variance S(2,2) (SV_S(2,2)), Correlat_S(0,2) Correlat_S(1,0), and SE_S(1,0) from Co-occurrence matrix; SRE_45Dgr and RLNU_Vert from Run-Length matrix and (Tab. 2).

ELs vs. PBHs

Eighteen texture features showed significant difference between NELs and PBHs: Difference Variance S(0,1) (DV_S(0,1)), DV_S(2,2), DV_S(0,4), Correlat_S(1,1), Correlat_S(1,–1), Correlat_S(1,0), SA_S(4,0), SE_S(1,0) and Angular Second Moment S(0,1) (ASM_S(0,1)) from Co-occurrence matrix; Gr_nonzeros and Gr_ Kurtosis from Gradient; WavEnHL_s-1, WavEnLH_s-1, WavEnLL_s–2, WavEnHL_s-2, WavEnLL_s-3 from Wavelet; SRE_45Dgr from Run-length matrix and Mean from Histogram (Tab. 3).

Briefly, the SE and DV measure any disorder or complexity and heterogeneity of an image. The correlation feature is a measure of gray-level linear dependencies in the image. SA represents the mean of gray-level image in the spatial domain. ASM measures textural uniformity. High value occurs when the gray-level distribution has a constant. SRE measures distribution of short runs and would occur more often in a fine texture. RLNU measures similarity of run lengths within the image. The RLNU is expected small if the run lengths are not similar. Gr_nonzeros measures percentage of pixels with non-zero gradient.

Area under the ROC curve for classification of ELs, NELs and PBHs

ROC analysis indicated that texture features of Co-occurrence matrix (Correlat_S(1,–1) and ASM_S(5,0)) and Wavelet (WavEnHH_s–1) had the highest A_z values in terms of difference between NELs and ELs. The A_z value of Correlat_S(1,-1), ASM_S(5,0) and WavEnHH_s-1 were 0.870, 0.868 and 0.859, respectively (Tab. 1).

The A_z values of texture features of Wavelet (WavEnLL_s-2, A_z = 0.794) and Histogram (Mean, A_z = 0.776) were higher than others in terms of difference between NELs and PBHs. The A_z values of each significant feature are listed in Tab. 2.

Texture features of Co-occurrence matrix (DV_S(0,1) and Correlat_S(1,1)) had higher A_z values in terms of difference between ELs and PBHs. The A_z value of DV_S(0,1) and Correlat_S(1,1) were 0.833 and 0.831, respectively (Tab. 3).

Texture analysis and classification

Diagnostic performance of the MPTA for classification and comparison between the NEL and PBH groups are shown in Tab. 4. Fig. 3 shows ROC curves of the proposed MPTA that demonstrate excellent performance in terms of classification between ELs and PBHs and between ELs and NELs with A_z = 1 that corresponds to sensitivity, specificity and accuracy of 100% (Tab. 4). Discrimination power was achieved with A_z value of 0.975, corresponding to sensitivity of 94.3%, specificity 96.3% and accuracy 95.5% (Fig. 3).

Discrimination distributions for LDA are illustrated in the majority of discriminating features direction and show that LDA had the greatest power to discriminate between ELs and PBHs and between ELs and NELs (Fig. 4).

Discussion

Discrimination between ELs, NELs and PBHs is one of the most critical factors to improve the initial diagnosis and therapy. The primary objective of this study was to evaluate texture ability as a non-invasive method to distinguish between NELs, ELs and PBHs. Results of comparisons showed a significant difference in terms of texture features between the three groups. The results of this study demonstrated that the TA was highly accurate in differentiating NELs (or PBHs) from ELs and NELs from PBH. The best results were driven with A_z of 1 in differentiating between NELs (or PBHs) and ELs (Fig. 3).

In general, according to the A_z-value, Co-occurrence matrix features had higher performance than other feature groups in terms of differentiation between NELs (or PBHs) and EL but Wavelet features had an advantage over the other feature groups in terms of differentiation between NELs and PBHs. The highest performance in classification was achieved by the Co-occur-

Tab. 2. Summary of performance for significant texture features in classification of NELs and PBHs and the associated P-values.

Texture Features	Post Hoc Tests (P-value)	A_z value[a]
WavEnLL_s-2	P < 0.001	0.794 (0.693, 0.894)
Mean	P < 0.001	0.776 (0.671, 0.881)
Gr_nonzeros	P = 0.006	0.767 (0.665, 0.869)
SA_S(3–3)	P < 0.001	0.767 (0.660, 0.875)
WavEnLL_s-1	P < 0.001	0.759 (0.693, 0.897)
SA_S(3,3)	P < 0.001	0.756 (0.647, 0.865)
SA_S(3,0)	P < 0.001	0.740 (0.627, 0.853)
Correlat_S(0,2)	P = 0.037	0.680 (0.565, 0.796)
SRE_45Dgr	P = 0.042	0.666 (0.552, 0.779)
SE_S(1,0)	P = 0.029	0.660 (0.547, 0.773)
SV_S(2,2)	P = 0.027	0.631 (0.516, 0.746)
RLNU_Vert	P = 0.025	0.631 (0.514, 0.748)
Correlat_S(1,0)	P = 0.439	0.626 (0.511, 0.741)
WavEnLH_s-2	P = 0.001	0.608 (0.478, 0.739)

A_z – area under ROC curve; WavEnLL and WavEnLH – 'low-low' and 'low-high' energy components in wavelet decomposition respectively; Gr_nonzeros – non-zero gradient matrix; SA – sum average; SRE_45Dgr – short sun emphasis in 45-degree direction; SE – sum entropy; SV – sum variance; RLNU_Vert – run length non-uniformity in vertical direction; [a] numbers in parentheses are 95% CI

Tab. 3. Summary of performance for significant texture features in classification of ELs and PBHs and the associated P-values.

Texture Features	Post Hoc Tests (P-value)	A_z value[a]
DV_S(0,1)	P < 0.001	0.833 (0.724, 0.942)
Correlat_S(1,1)	P < 0.001	0.831 (0.720, 0.942)
DV_S(2,2)	P = 0.001	0.816 (0.704, 0.927)
Gr_ Kurtosis	P = 0.011	0.813 (0.701, 0.924)
ASM_ S(0,1)	P < 0.001	0.794 (0.672, 0.915)
Correlat_S(1,-1)	P < 0.001	0.792 (0.679, 0.904)
Mean	P = 0.001	0.759 (0.611, 0.906)
WavEnLH_s-1	P < 0.001	0.739 (0.610, 0.867)
SA_S(4,0)	P < 0.001	0.739 (0.589, 0.888)
WavEnHL_s-1	P = 0.006	0.737 (0.608, 0.865)
DV_S(0,4)	P = 0.030	0.733 (0.607, 0.859)
SE_S(1,0)	P = 0.001	0.726 (0.579, 0.873)
WavEnHL_s-2	P=0.004	0.723 (0.593, 0.853)
Correlat_S(1,0)	P = 0.008	0.723 (0.593, 0.852)
WavEnLL_s-2	P = 0.002	0.710 (0.552, 0.868)
WavEnLL_s-3	P = 0.001	0.696 (0.537, 0.856)
SRE_45Dgr	P = 0.006	0.683 (0.532, 0.833)
Gr_nonzeros	P < 0.001	0.680 (0.523, 0.838)

A_z – area under ROC curve; DV – difference variance; Gr_Kurtosis – kurtosis of absolute gradient; ASM – Angular Second Moment; WavEnLH, WavEnHL and WavEnLL – 'low-high', 'high--low' and 'low-low' energy components in wavelet decomposition respectively; SA – sum average; SE – sum entropy; SRE_45Dgr – short sun emphasis in 45-degree direction; Gr_nonzeros – non-zero gradient matrix; [a] numbers in parentheses are 95% CI.

Tab. 4. Diagnostic performance of proposed computer aided diagnostic system for classification of NELs, ELs and PBHs.

Group	SEN (%)	SPC (%)	ACC (%)	A_z value[a]	Correct Classification
NEL vs. PBH	94.3	96.3	95.5	0.975 (0.950, 1)	85/89 (95.5%)
NEL vs. EL	100	100	100	1	81/81 (100%)
EL vs. PBH	100	100	100	1	62/62 (100%)

SEN – sensitivity; SPC – specificity; ACC – accuracy; PPV – positive predictive value; NPV – negative predictive value; A_z – area under ROC curve; [a] – numbers in parentheses are 95% CI.

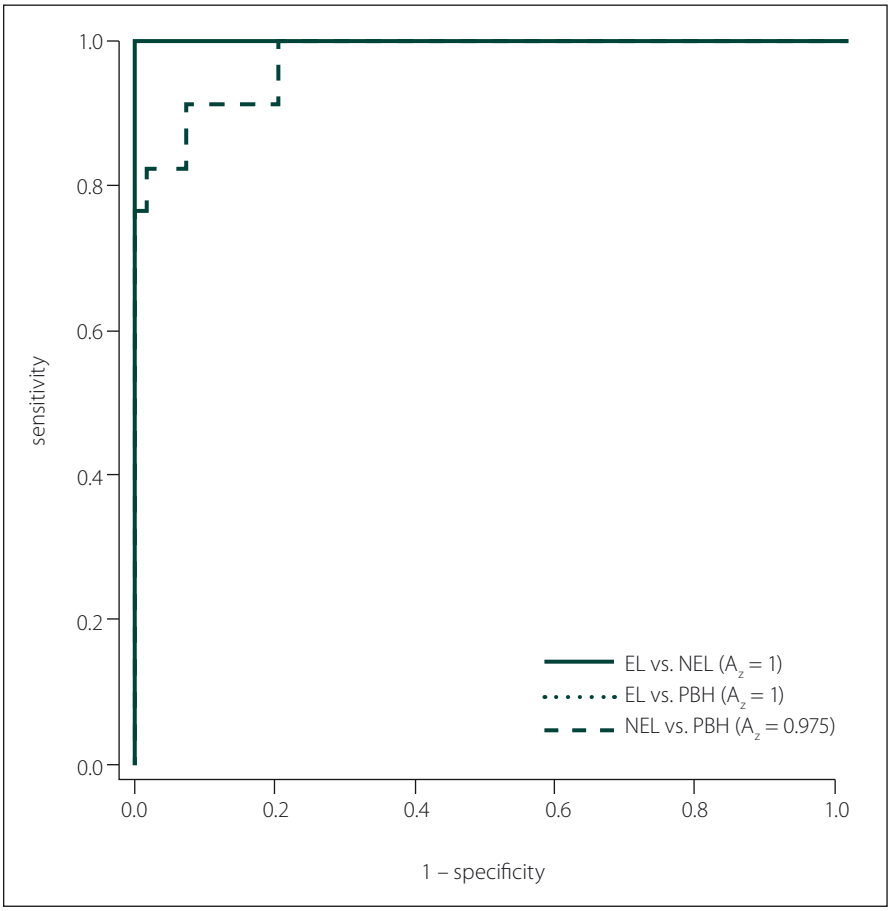

Fig. 3. The ROC curve diagrams for texture analysis with LDA in classification of NELs, ELs and PBHs.

rence matrix based feature (Correlat_S(1,-1)) with $A_z = 0.870$. Among the texture features, there was a significant difference between the three groups and Run-length matrix features were less sensitive than the others as the features groups had a lower A_z-value (ranging from 0.631 to 0.766).

A_z values ordered by LDA using all significant texture features had a higher level of performance than each of the texture features alone to classification groups. In this regard, A_z value of LDA in classification NELs and PBHs were 0.975 and this corresponded to sensitivity of 94.3%, specificity of 96.3% and accuracy of 95.5%, while the highest level of performance was achieved by WavEnLL_s-2 with $A_z = 0.794$. LDA yielded excellent performance in classifying NELs from ELs and PBHs from ELs with $A_z = 1$, while the highest performance achieved by Correlat_S(1,–1) and DV_S(0,1) were the A_z value of 0.870 and 0.833, respectively.

Based on significant texture features, EL had a higher Mean (or intensity) than PBH and NEL on T2WI. These differences arise from the result of demyelination and increased water content of the lesions and ineffective spin-spin interaction. The result of this ineffective interaction caused increased T2 relaxation time and intensity. It has been shown that tissue-relaxation rates in pre-contrast injection phase showed significant differences between ELs and NELs as ELs having a higher mean transverse relaxation rate and so appeared brighter in T2WI [30]. Our study confirmed this result by using TA that did not require measurement of tissue--relaxation rate. On the other hand, results indicate that texture features based on Gradient, Co-occurrence matrix and Wavelet, EL had less heterogeneity in pixel intensity distribution than PBH (or NEL) and PBH had less heterogeneity than NEL on T2WI. On the other hand, according to the Run-length matrix based features, EL had finer texture than PBH (or NEL) and PBH had finer texture than NEL on T2WI. Several studies have evaluated texture features for differentiation of lesions in MS subjects. In this regard, dynamic texture parameter analysis (DTPA) was used to detect pathological changes between ELs and NELs by dynamic susceptibility contrast-enhanced imaging. It has been shown that the first order texture features in DTPA were useful for differentiation of NELs and ELs [19,20]. Yu et al. examined 8 texture features (5 Run-length matrix and 3 Histogram features) to differentiate 9 ELs and 23 NELs with 100% accuracy [21].

Zhang et al. indicated that TA based on Polar Stockwell transform were useful to find differences between persist and transient acute black holes using conventional T1WI [22]. In this study, first and second (or high) order texture features such as Run-length matrix, Co-occurrence matrix and Wavelet features were used to detect subtle differences in ELs, NELs and PBHs in conventional T2WIs.

Researches in recent years have indicated that advanced MRI techniques have significantly improved conventional MRI techniques [31]. In this regards, magnetization transfer imaging, Diffusion Tensor Imaging, proton MRI spectroscopy have the capacity to discern between ELs and NELs (or PBHs) [30, 32–35]. However, up till now,

advanced MRI techniques have not been routinely implemented in imaging centers. The results of this study indicate that TA can improve our understanding of the MS disease from conventional MRI images.

New lesions at follow-up scans that imply activity may need therapy switch [25]. Contrast agents require additional time and cost and can cause discomfort for patients during administration and MRI imaging. Gadolinium-based contrast agents (GBCA) are widely used in MRI imaging due to their paramagnetic properties. It has been used to evaluate the MS plaque activity by increasing signal intensity on T1WIs. Inflammation in MS can disrupt blood brain barrier. Hence, gadolinium accumulation is proportional to a plaque activity, as it more intensively accumulates in new active plaques. Although recent researches have indicated that signal intensity of dentate nucleus and the globus pallidus on unenhanced T1WIs can increase after multiple administrations and correlated with the number of administrations [36–38] and this can leads to misunderstanding in interpretation of MR images. Also, according to the U.S. Food and Drug Administration (FDA), although there have been no reports of signs of central nervous system toxicity based on GBCA, every precaution should be taken to reduce the potential for gadolinium accumulation. In this regard, gadolinium use should be limited [39]. It is desirable to introduce a method to identify and characterize active MS lesions without administration of a contrast agent. The results of this study showed that TA provided useful information and had the potential to characterize EL in T2WI MRI sequence and save time and costs.

In this study, some limitations should be clearly noted. First, the data group was small, further investigation with a larger data set is needed. Second, ROI was selected manually, further investigation can be equipped with automated, or semi-automated ROI selection. Third, subjects could have been positioned differently during the process of image acquisition. Since the magnetic field is non-uniform along MRI system magnet, textural features of tissue may be different. Fourth, patients with a history of neurological symptoms suggestive of demyelination were excluded. Finally, in this study, we just indicated that texture analysis can differentiate between three types of MS lesions. Further study is needed to examine lesion types in a prospective approach.

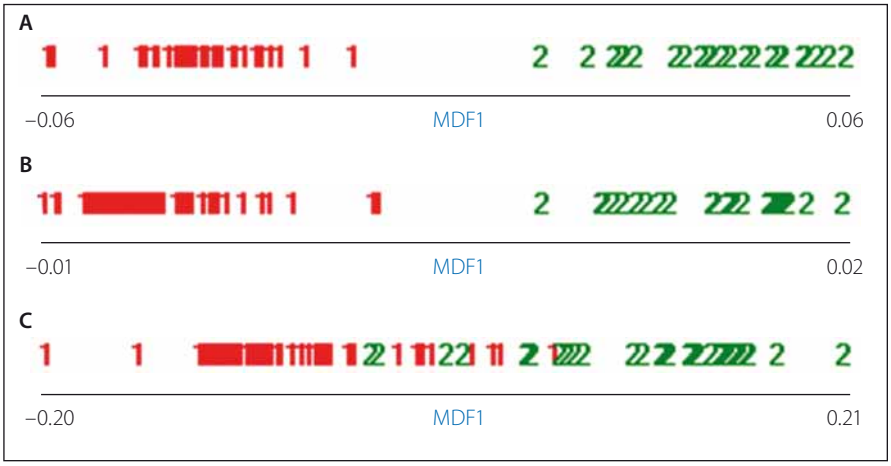

Fig. 4. Sample distributions after texture analysis, LDA: NELs and ELs (A); ELs and PBHs (B); NELs and PBHs (C). MDF: Most discriminating features; "1" represents NEL in (A) and (C), "2" represents EL in (A) and (B). "1" represents "2" represents PBH in (B) and (C) respectively.

Conclusion

Generally, our results indicate that TA is a useful tool for discrimination of ELs, NELs and PBHs by a conventional MRI sequence. The main advantage of this method is that it can be an auxiliary tool to improve diagnostic accuracy and to provide new insights into lesions using conventional MRI sequences. Furthermore, it incurs no additional cost, pulse sequences or scanning time. TA can be an auxiliary tool to help physicians improve their understanding of MS pathophysiology in conventional MRI sequences.

References

1. Compston A, Coles A. Multiple sclerosis. Lancet 2002;359(9313):1221–31. doi: 10.1016/S0140-6736(02)08220-X.

2. Young I, Hall A, Pallis C, et al. Nuclear magnetic resonance imaging of the brain in multiple sclerosis. The Lancet 1981;318(8255):1063–6.

3. Thompson A, Montalban X, Barkhof F, et al. Diagnostic criteria for primary progressive multiple sclerosis: a position paper. Ann Neurol 2000;47(6):831–5.

4. Sahraian MA, Eshaghi A. Role of MRI in diagnosis and treatment of multiple sclerosis. Clin Neurol Neurosurg 2010;112(7):609–15. doi: 10.1016/j.clineuro.2010.03.022

5. Rovira À, Auger C, Alonso J. Magnetic resonance monitoring of lesion evolution in multiple sclerosis. Therapeutic advances in neurological disorders 2013;6(5):298–310. doi: 10.1177/1756285613484079.

6. Zivadinov R, Bakshi R. Role of MRI in multiple sclerosis II: brain and spinal cord atrophy. Front Biosci 2004;9:647–64. doi: 10.2741/1262.

7. Filippi M, Rovaris M, Rocca M, et al. Glatiramer acetate reduces the proportion of new MS lesions evolving into "black holes". Neurology 2001;57(4):731–3. doi: 10.1212/WNL.57.4.731.

8. Sahraian M, Radue EW, Haller S, et al. Black holes in multiple sclerosis: definition, evolution, and clinical correlations. Acta Neurol Scand 2010;122(1):1–8. doi: 10.1111/j.1600-0404.2009.01221.x.

9. Tam R, Traboulsee A, Riddehough A, et al. The impact of intensity variations in T1-hypointense lesions on clinical correlations in multiple sclerosis. Multiple Sclerosis Journal 2011;17(8):949–57. doi: 10.1177/1352458511402113.

10. van Waesberghe J, Kamphorst W, De Groot CJ, et al. Axonal loss in multiple sclerosis lesions: magnetic resonance imaging insights into substrates of disability. Ann Neurol 1999;46(5):747–54.

11. Ardakani AA, Gharbali A, Saniei Y, et al. Application of texture analysis in diagnosis of multiple sclerosis by magnetic resonance imaging. Glob J Health Sci 2015;7(6):68–78. doi: 10.5539/gjhs.v7n6p68.

12. Materka A. Texture analysis methodologies for magnetic resonance imaging. Dialogues Clin Neurosci 2004;6(2):243–50.

13. Materka A, Strzelecki M. Texture analysis methods – A review. Brussels: Technical University of Lodz 1998.

14. Fazekas F, Barkhof F, Filippi M, et al. The contribution of magnetic resonance imaging to the diagnosis of multiple sclerosis. Neurology 1999;53(3): 448–56. doi: 10.1212/WNL.53.3.448.

15. Zhang J, Tong L, Wang L, et al. Texture analysis of multiple sclerosis: a comparative study. Magn Reson Imaging 2008;26(8):1160–6. doi: 10.1016/j.mri.2008.01.016.

16. Harrison LC, Raunio M, Holli KK, et al. MRI texture analysis in multiple sclerosis: toward a clinical analysis protocol. Acad Radiol 2010;17(6):696–707. doi: 10.1016/j.acra.2010.01.005.

17. Loizou CP, Murray V, Pattichis MS, et al. Multiscale amplitude-modulation frequency-modulation (AM–FM) texture analysis of multiple sclerosis in brain MRI images. IEEE Trans Inf Technol Biomed 2015;15(1):119–29. doi: 10.1109/TITB.2010.2091279.

18. Michoux N, Guillet A, Rommel D, et al. Texture Analysis of T2-Weighted MR Images to Assess Acute Inflammation in Brain MS Lesions. PloS one 2015;10(12):e0145497. doi: 10.1371/journal.pone.0145497.

19. Verma RK, Slotboom J, Heldner MR, et al. Characterization of microcirculation in multiple sclerosis lesions by dynamic texture parameter analysis (DTPA). PloS one 2013;8(7):e67610.doi: 10.1371/journal.pone.0067610.

20. Verma RK, Slotboom J, Locher C, et al. Characterization of Enhancing MS Lesions by Dynamic Texture Parameter Analysis of Dynamic Susceptibility Perfusion Imaging. Biomed Res Intl 2016. doi: 10.1155/2016/9578139.

21. Yu O, Mauss Y, Zollner G, et al. Distinct patterns of active and non-active plaques using texture analysis on brain NMR images in multiple sclerosis patients: preliminary results. Magn Reson Imaging 1999;17(9):1261–7. doi: 10.1016/S0730-725X(99)00062-4.

22. Zhang Y, Traboulsee A, Zhao Y, et al. Texture analysis differentiates persistent and transient T1 black holes at acute onset in multiple sclerosis: a preliminary study. Mult Scler 2011;17(5):532–40. doi: 10.1177/1352458510395981.

23. Texture analysis of MR images of minocycline treated MS patients. International Conference on Medical Image Computing and Computer-Assisted Intervention; 2003. Springer. doi: 10.1007/978-3-540-39899-8.

24. Zhang Y, Moore G, Laule C, et al. Pathological correlates of magnetic resonance imaging texture heterogeneity in multiple sclerosis. Ann Neurol 2013;74(1):91–9. doi: 10.1002/ana.23867.

25. Polman CH, Reingold SC, Banwell B, et al. Diagnostic criteria for multiple sclerosis: 2010 revisions to the McDonald criteria. Ann Neurol 2011;69(2):292–302. doi: 10.1002/ana.22366.

26. Ben-Zacharia A. The Effect of Modifiable Risk Factors on Multiple Sclerosis Progression (P1.387). Neurology 2016;86(16 Suppl):P1. 387.

27. Bitsch A, Bruck W. MRI-pathological correlates in MS. International MS Journal 2002;8(3):88–95

28. Castellano G, Bonilha L, Li LM, et al. Texture analysis of medical images. Clin Radiol 2004;59(12):1061–9. doi: 10.1016/j.crad.2004.07.008.

29. Van Erkel AR, Pattynama PMT. Receiver operating characteristic (ROC) analysis: basic principles and applications in radiology. Eur J Radiol 1998;27(2):88–94. doi: 10.1016/S0720-048X(97)00157-5.

30. Blystad I, Håkansson I, Tisell A, et al. Quantitative MRI for Analysis of Active Multiple Sclerosis Lesions without Gadolinium-Based Contrast Agent. Am J Neuroradiol 2016;37(1):94–100. doi: 10.3174/ajnr.A4501.

31. Rovira À, Wattjes MP, Tintoré M, et al. Evidence--based guidelines: MAGNIMS consensus guidelines on the use of MRI in multiple sclerosis [mdash] clinical implementation in the diagnostic process. NatRevNeurol2015;11(8):471–82.doi:10.1038/nrneurol.2015.106.

32. Abdoli M, Chakraborty S, MacLean HJ, et al. The evaluation of MRI diffusion values of active demyelinating lesions in multiple sclerosis. Mult Scler Relat Disord 2016;10:97–102. doi: 10.1016/j.msard.2016.09.006.

33. Faizy TD, Thaler C, Kumar D, et al. Heterogeneity of Multiple Sclerosis Lesions in Multislice Myelin Water Imaging. PLoS One 2016;11(3):e0151496. doi: 10.1371/journal.pone.0151496.

34. Srinivasan R, Sailasuta N, Hurd R, et al. Evidence of elevated glutamate in multiple sclerosis using magnetic resonance spectroscopy at 3 T. Brain 2005;128(5):1016–25. doi: 10.1093/brain/awh467.

35. Stagg C, Rothman DL. Magnetic resonance spectroscopy: tools for neuroscience research and emerging clinical applications. Cambridge, Massachusetts: Academic Press 2013.

36. Radbruch A, Weberling L, Kieslich P, et al. Gadolinium retention in the dentate nucleus and globus pallidus is dependent on the class of contrast agent. Radiology 2015;275(3):783–91. doi: 10.1148/radiol.2015150337

37. Conte G, Preda L, Cocorocchio E, et al. Signal intensity change on unenhanced T1-weighted images in dentate nucleus and globus pallidus after multiple administrations of gadoxetate disodium: an intraindividual comparative study. Eur Radiol 2017:1–7 doi: 10.1007/s00330-017-4810-3.

38. Stojanov D, Aracki-Trenkic A, Vojinovic S, et al. Increasing signal intensity within the dentate nucleus and globus pallidus on unenhanced T1W magnetic resonance images in patients with relapsing-remitting multiple sclerosis: correlation with cumulative dose of a macrocyclic gadolinium-based contrast agent, gadobutrol. Eur Radiol 2016;26(3):807–15. doi: 10.1007/s00330-015-3879-9.

39. Food U, Administration D. FDA drug safety communication: FDA evaluating the risk of brain deposits with repeated use of gadolinium-based contrast agents for magnetic resonance imaging (MRI), 2015.